PROCEEDINGS OF SCIENCE

ONLINE ICRC 2021
THE ASTROPARTICLE PHYSICS CONFERENCE
Berlin | Germany
37th International Cosmic Ray Conference
12–23 July 2021

Event-by-event reconstruction of the shower maximum $X_{\mathbf{max}}$ with the Surface Detector of the Pierre Auger Observatory using deep learning

Jonas Glombitza[a,*] **on behalf of the Pierre Auger**[b] **Collaboration**
(a complete list of authors can be found at the end of the proceedings)

[a] *III. Physics Institute A, RWTH Aachen University, Aachen, Germany*
[b] *Observatorio Pierre Auger, Av. San Martín Norte 304, 5613 Malargüe, Argentina*
E-mail: spokespersons@auger.org

The measurement of the mass composition of ultra-high energy cosmic rays constitutes a prime challenge in astroparticle physics. Most detailed information on the composition can be obtained from measurements of the depth of maximum of air showers, X_{max}, with the use of fluorescence telescopes, which can be operated only during clear and moonless nights.
Using deep neural networks, it is now possible for the first time to perform an event-by-event reconstruction of X_{max} with the Surface Detector (SD) of the Pierre Auger Observatory. Therefore, previously recorded data can be analyzed for information on X_{max}, and thus, the cosmic-ray composition. Since the SD operates with a duty cycle of almost 100% and its event selection is less strict than for the Fluorescence Detector (FD), the gain in statistics with respect to the FD is almost a factor of 15 for energies above $10^{19.5}$ eV.
In this contribution, we introduce the neural network particularly designed for the SD of the Pierre Auger Observatory. We evaluate its performance using three different hadronic interaction models, verify its functionality using Auger hybrid measurements, and find that the method can extract mass information on an event level.

37th International Cosmic Ray Conference (ICRC 2021)
July 12th – 23rd, 2021
Online – Berlin, Germany

*Presenter

PoS(ICRC2021)359

1. Introduction

Measuring the mass composition of ultra-high energy cosmic rays (UHECRs) provides insights into cosmic-ray acceleration and propagation. Beyond this, composition estimates on an event level could enable new analysis techniques for the search for cosmic-ray sources. However, the reconstruction of mass-sensitive information of UHECRs at the Pierre Auger Observatory [1] on an event-level is currently confined to fluorescence observations [2, 3], with their limited duty cycle.

In recent years, several strategies were developed to reconstruct mass information using the Surface Detector (SD) to increase the event statistics by a factor of 25 above 3 EeV (12 beyond 30 EeV) when compared to the Fluorescence Detector (FD). Using the phenomenological approach of shower universality [4] information on the mass composition can be reconstructed by decomposing the measured signals into the shower components. Recently, promising results were obtained for determining $X_{\max}$ with good accuracy [5, 6]. The so-called 'delta method' that was extensively studied in the past is based on the rise times of the recorded signals and can measure the average composition of UHECRs accurately from 0.3 EeV to 100 EeV [7, 8]. Nevertheless, a more precise measurement beyond the average composition has not yet been possible.

The approach discussed in this work is aimed to exploit mass-sensitive information beyond the average composition on an event-by-event basis. Our technique to reconstruct $X_{\max}$ from the SD data is based on the deep neural network (DNN) developed in [9] and recently tailored to the conditions of the Pierre Auger Observatory [10]. In this contribution, the potential of this method for determining mass information on an event level will be examined in detail.

2. Data

The SD registers the time-dependent signals induced by air-shower particles traversing water-Cherenkov detectors (WCDs). Using three photomultiplier tubes (PMTs), three signal traces are recorded in time steps of 25 ns. By adopting a dedicated algorithm to suppress backgrounds, the starting time of the signal trace can be determined [11]. For each WCD this results in a characteristic arrival time of the first shower particles and three cleaned signal traces, which are further trimmed to 3 μs (120 time steps). By means of a local calibration, the signals are converted to a multiple of the signal from a vertical equivalent muon (VEM) — the signal a single muon induces when traversing a WCD vertically.

2.1 Simulation libraries

For simulation studies, we use air showers simulated using CORSIKA [12] and the hadronic interaction models EPOS-LHC [13], QGSJetII-04 [14], and Sibyll 2.3 [15]. The detector responses were simulated using Geant4 [16] and the Offline framework [17] of the Pierre Auger Observatory. Each of these three data sets consists of hydrogen, helium, oxygen, and iron showers in equal fractions. The simulated energies follow a spectrum of E^{-1} and range from 1 to 160 EeV. The showers are uniformly distributed in azimuth angle and follow a zenith-angle distribution that ranges from 0° to 65° and is flat in $\cos^2\theta$. In total, each simulated data set contains 450,000 events. For training the network, we use 400,000 events of the EPOS-LHC data set and leave 50,000 for evaluation. The data sets of QGSJetII-04 and Sibyll 2.3 are entirely used for evaluation. In contrast

to training, we evaluate the DNN in an energy range of 3 EeV to 100 EeV and a zenith range of $0^\circ \leq \theta < 65^\circ$, since in this phase space, the SD ensures particularly reliable reconstructions [11].

2.2 Hybrid measurements

For verifying and calibrating the DNN, we prepare a data set of hybrid measurements with event reconstructions from the SD and the FD. For a detailed description of the hybrid selection and reconstruction, refer to [2]. In this work, we use events measured between 1 January 2004 and 31 December 2017 with energies larger than 3.16 EeV, as measured by the SD. We further discard events with an inactive WCD station in the first hexagon around the station with the largest signal, and events that feature bad calibration values. In summary, 3,109 events remain after the selection.

2.3 Pre-processing

Pre-processing of data is crucial for training neural networks and is briefly discussed below. To process the recorded footprint, we use for each event a cutout of 13×13 stations, centered at the station with the largest signal. This significantly reduces the memory consumption since almost all events have smaller footprints. Further, we re-scale each measured signal traces $S_i(t)$ using:

$$\tilde{S}_i(t) = \frac{\log_{10}[S_i(t)/\mathrm{VEM} + 1]}{\log_{10}[S_{\mathrm{norm}} + 1]}, \tag{1}$$

where $S_{\mathrm{norm}} = 100$ is used to normalize signals of 100 VEM to 1. In addition, the arrival times are standardized with respect to τ_{center}, the arrival time of the station with the largest signal, using:

$$\tilde{t}_{0,i} = \frac{t_{0,i} - \tau_{\mathrm{center}}}{\sigma_{t,\mathrm{train\ data}}} \tag{2}$$

Here, $\sigma_{t,\mathrm{train\ data}}$ denotes the standard deviation of the distribution of arrival times calculated over the entire training data set.

3. Deep-learning based reconstruction

The DNN used here is based on state-of-the-art machine learning techniques and can be roughly divided into two parts. The first part of the network utilizes recurrent networks (Long-Short Term Memory [18]) to process the signal traces measured by each WCD. In the second part, space- and time-dependent information is analyzed using hexagonal convolutions [19] to exploit the hexagonal structure of the SD array. The network is implemented using Keras [20] and TensorFlow [21].

3.1 Training

For training the network, we used 400,000 showers simulated with EPOS-LHC. During the training, we used an on-the-fly augmentation of data that mimics realistic but changing operating conditions of the observatory, such as failures of PMTs or WCDs. As an objective function, we chose the mean squared error that is minimized separately for each of the four elements. We trained the DNN for 150 epochs with a batch size of 48, which took roughly 60 h on an NVIDIA GeForce GTX 1080 GPU. For more details on the network architecture and the training strategy, see [10].

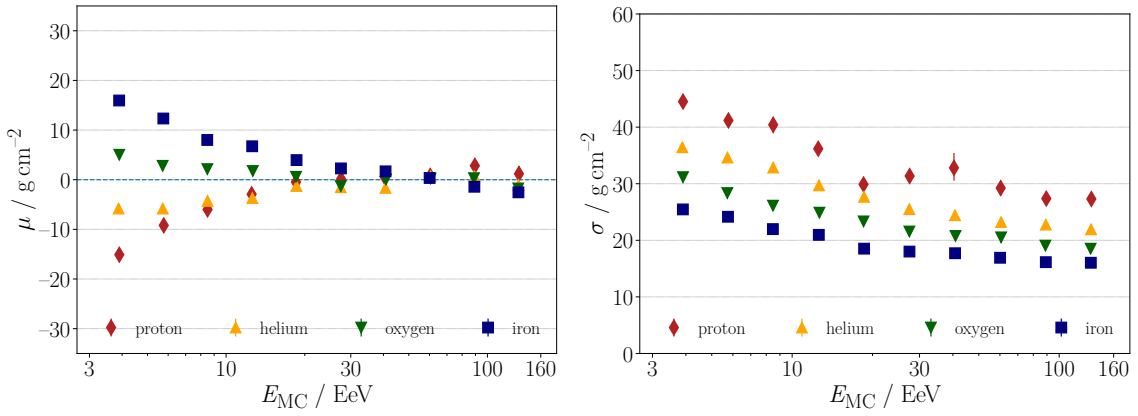

(a) EPOS-LHC **(b)** EPOS-LHC

Figure 1: Energy-dependent (a) bias ($\mu = X_{\mathrm{max,DNN}} - X_{\mathrm{max,MC}}$) and (b) resolution of the DNN evaluated on EPOS-LHC showers. The DNN was trained using EPOS-LHC showers. Different colors indicate different primary species.

4. Performance on simulations

In the following, the performance of the network trained on EPOS-LHC is evaluated using air showers simulated using the hadronic interaction models EPOS-LHC, QGSJetII-04, and Sibyll 2.3. In Fig. 1 the $X_{\max}$ reconstruction performance — the bias and resolution of the DNN — is shown as a function of energy for showers simulated using EPOS-LHC for a pure proton, helium, oxygen, and iron composition. Statistical uncertainties, denoted by vertical bars, are mostly hidden by the markers and were obtained using bootstrapping. As visible in Fig. 1a, below 10 EeV the reconstruction exhibits a moderate composition bias ($\mu = X_{\mathrm{max,DNN}} - X_{\mathrm{max,MC}}$). Here, on average $X_{\max}$ is reconstructed too shallow for proton and helium showers and too deep for oxygen and iron showers. Beyond 10 EeV, the composition bias diminishes and is below ± 5 g/cm^2. When averaging over all compositions, the overall bias vanishes.

The energy-dependent resolution of the method on EPOS-LHC showers, as shown in Fig. 1b, is composition-dependent and improves with increasing energy and particle mass. This dependency is expected, as for larger energies larger footprints are induced on the SD, and for increasing mass, the shower-to-shower fluctuations decrease. At 3 EeV, the resolution for reconstructing protons (iron) is 45 g/cm^2 (25 g/cm^2) and improves to roughly 30 g/cm^2 (15 g/cm^2) at 100 EeV.

The evaluation of the $X_{\max}$ reconstruction using showers simulated with a different hadronic interaction model than used for training is shown in Fig. 2. When investigating the energy-dependent bias of the reconstruction (compare Fig. 2a and Fig. 2c), a composition bias can be found, which is similar to the composition bias seen in Fig. 1a. However, an overall bias — when averaging over the composition — can be observed, which depends slightly on the energy. At higher energies, this shift amounts to roughly -5 g/cm^2 for showers simulated using the QGSJetII-04 and roughly -15 g/cm^2 for Sibyll 2.3 showers.

In contrast, the event-by-event resolution is similar to the results obtained using EPOS-LHC. It amounts to roughly 40 g/cm^2 (20 g/cm^2) at 10 EeV for protons (iron) and improves with increasing

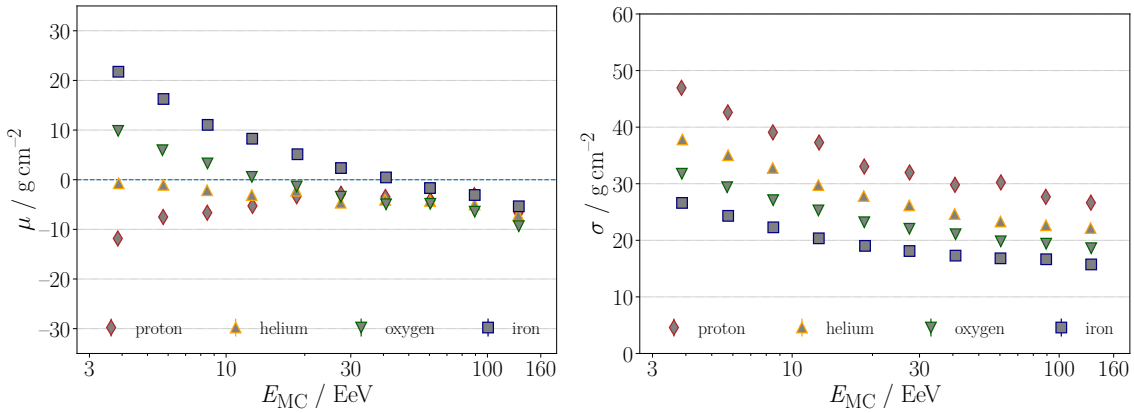

(a) QGSJetII-04 **(b)** QGSJetII-04

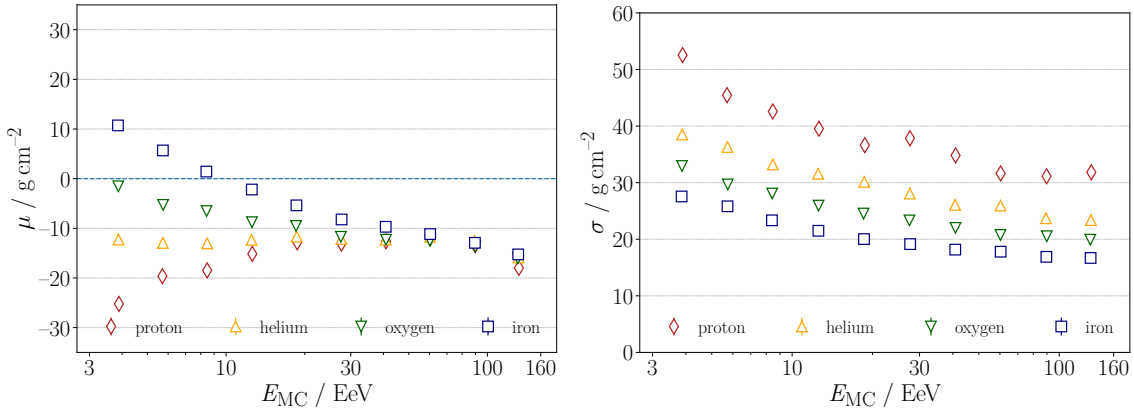

(c) Sibyll 2.3 **(d)** Sibyll 2.3

Figure 2: Evaluation of the DNN trained using EPOS-LHC showers. Energy-dependent bias (left) and resolution (right) when evaluating the DNN with showers simulated using QGSJetII-04 (top), and Sibyll 2.3 (bottom). Different colors indicate different primary species.

energy to 30 g/cm^2 (15 g/cm^2) (compare Fig. 2b and Fig. 2d).

To conclude, the event-by-event resolution is independent of the hadronic model. In contrast, the $X_{\max}$ scale of the DNN depends on the hadronic model, which implies that a calibration of the method is required. A calibration of the DNN to the $X_{\max}$ scale of the FD is discussed in Section 5.

4.1 Separation of protons and iron nuclei

To assess the suitability of an estimator to perform mass-composition studies on an event level, a so-called *merit factor* can be used, which estimates the discrimination power between two primary species. The merit factor for discriminating between iron nuclei and protons is given by

$$f_{\mathrm{MF}} = \frac{|\langle X_{\max,\mathrm{P}}\rangle - \langle X_{\max,\mathrm{Fe}}\rangle|}{\sqrt{\sigma^2(X_{\max,\mathrm{P}}) + \sigma^2(X_{\max,\mathrm{Fe}})}}, \tag{3}$$

where $\langle X_{\max}\rangle$ denotes the mean and $\sigma(X_{\max})$ the standard deviation of the $X_{\max}$ distribution formed by protons or iron nuclei, respectively. Merit factors of 1.5 and larger correspond to a good

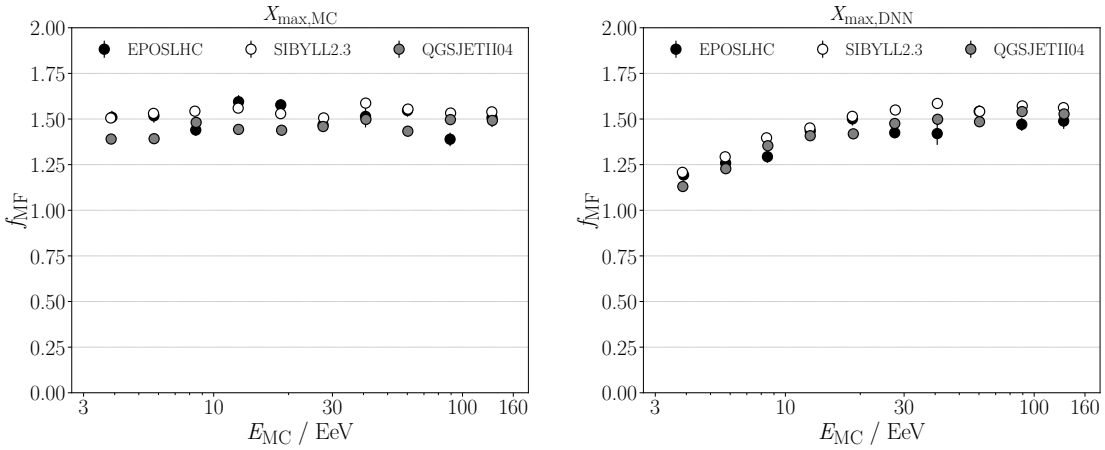

(a) Obtained using $X_{\max,\mathrm{MC}}$

(b) Obtained using $X_{\max,\mathrm{DNN}}$

Figure 3: Energy dependent merit factors for discriminating between proton and iron primaries using the (a) simulated (true) $X_{\max}$ and (b) the reconstructed $X_{\max}$ values of the DNN.

separation of the two primary masses and can be theoretically achieved using the true (simulated) $X_{\max}$ values, as shown in Fig. 3a.

For comparison, we show the energy-dependent merit factors using $X_{\max}$ reconstructions of the DNN in Fig. 3b for EPOS-LHC, QGSJetII-04, and Sibyll 2.3 showers. At 3 EeV, the merit factors amount to roughly 1.25, improve with increasing energy, and reach the theoretical limit of 1.5 at approximately 20 EeV. This finding indicates that after calibrating the DNN to the $X_{\max}$ scale of the FD (see below), it can be used to perform mass-composition studies on a single event level with excellent fidelity.

5. Application to hybrid data

To verify the reconstruction of the DNN and to calibrate the method to the $X_{\max}$ scale of the FD — which can be precisely determined [2] — we use golden hybrid events. Prior to comparing the $X_{\max}$ reconstructions of the DNN to FD observations, we correct the DNN reconstructions for detector ageing effects of the WCDs. This correction is described in detail in [10] and is based on information provided by detector monitoring [22].

In Fig. 4, we show the correlation between the $X_{\max}$ reconstruction of the FD and the DNN. The event-by-event correlation amounts to 0.63 and remains above 0.6 if we further correct $X_{\max}$ for the elongation rate as measured by the FD [2]. A bias of roughly -30 g/cm^2 can be observed, indicating that the DNN predictions are too shallow on average. A bias is expected since we observed a negative bias when evaluating the DNN on hadronic interaction models different to that used for the training (see Section 4). However, the size of the bias is larger than expected. One reason for this could be that the current generation of hadronic interaction models cannot describe the muonic component of air showers in full detail [7, 8, 23, 24].

This bias exhibits no significant dependency on the energy, as shown in Fig. 5a. Only the first bin deviates slightly from the observed bias of -30 g/cm^2, which may be caused by the increased

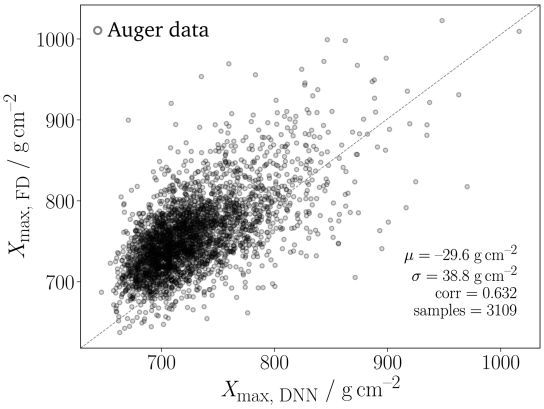

Figure 4: Event-by-event correlation of $X_{\max}$ as measured by the DNN and the FD using golden hybrids.

reconstruction bias at low energies (compare to Fig. 1a). After fitting a constant to the data, which yields -30.0 ± 0.6 g/cm^2, the predictions of the DNN are calibrated to the FD $X_{\max}$ scale.

We show the energy dependence of $\sigma(X_{\max,\mathrm{DNN}} - X_{\max,\mathrm{FD}})$ in Fig. 5b. Statistical uncertainties are estimated using bootstrapping. To extract the resolution of the DNN, we first parameterize this dependency by fitting the function $\sigma_{\Delta X_{\max}}(E) = a \cdot e^{-b \cdot (\log_{10} E/\mathrm{eV} - 18.5)} + c$ to the data. The obtained parameters are $a = 18.0 \pm 2.5$ g/cm^2, $b = 2.9 \pm 1.2$, and $c = 27.7 \pm 2.6$ g/cm^2. The fit is depicted as the continuous red line in Fig. 5b. To determine the resolution of the DNN, we subtract the FD resolution [2], which is shown as dashed grey line, in quadrature. The resulting DNN resolution is shown as a dashed red line. It improves from approximately 40 g/cm^2 at 3 EeV to below 25 g/cm^2 beyond 20 EeV. This is in good agreement with our expectations from simulation studies (compare with Fig. 2) and strengthens the finding that the resolution is independent of the interaction model. This implies that only a calibration to the $X_{\max}$ scale of the FD, as performed above, is needed for using the DNN for event-by-event composition studies.

6. Conclusion

In this contribution, we presented a deep neural network (DNN) to reconstruct the atmospheric depth of the shower maximum $X_{\max}$ using the SD. The network was trained using EPOS-LHC showers and further evaluated on QGSJetII-04 and Sibyll 2.3 showers. The composition bias of the reconstruction is similar for all interaction models and amounts to only a few g/cm^2 beyond 10 EeV. Additionally, it was found that the overall bias of the $X_{\max}$ reconstruction depends on the hadronic interaction model used, requiring a calibration of the method. In contrast, the resolution was found to be independent of the interaction model. It amounts for protons (iron) to roughly 40 g/cm^2 (25 g/cm^2) at 10 EeV, and reaches 30 g/cm^2 (15 g/cm^2) beyond 100 EeV. By further investigating the discrimination power of the reconstruction, it was shown that the DNN will enable mass-composition studies on an event level.

To verify the method's performance and calibrate the predictions of the DNN to the $X_{\max}$ scale of the FD, hybrid measurements were used. The calibration was found to be energy-independent, with a size of the $X_{\max}$ bias moderately above expectations from simulation studies. The resolution

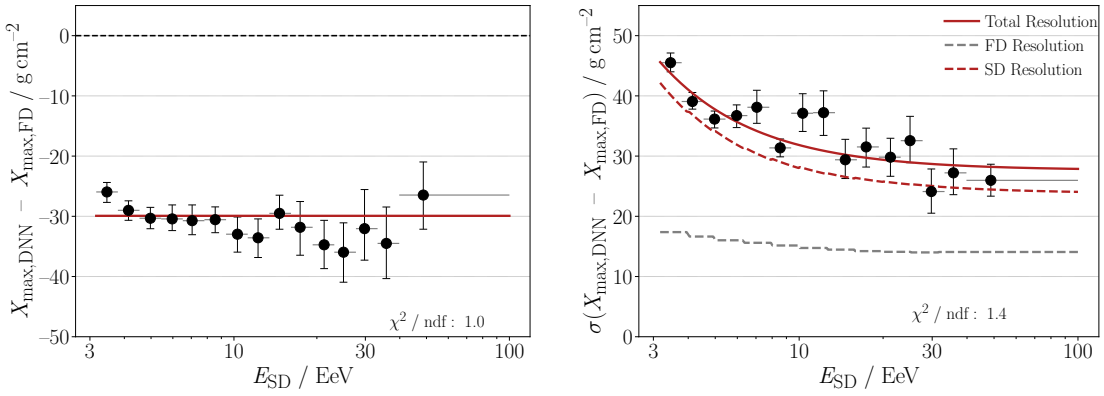

(a) Bias **(b)** Resolution

Figure 5: (a) Energy-dependent reconstruction bias of the DNN when compared to the FD. The calibration fit is shown as a continuous red line. (b) $\sigma(X_{\mathrm{max,DNN}} - X_{\mathrm{max,FD}})$ as a function of energy. Its fitted energy dependency is depicted as a continuous red line. The extracted resolution of the DNN is shown as a dashed red line after accounting for the resolution of the FD (dashed grey line).

extracted from data matches the expectations and improves from 40 g/cm^2 at 3 EeV to 25 g/cm^2 beyond 20 EeV. This will enable a precise measurement of the UHECR composition to the highest energies and give new prospects for composition-based analyses on an event level. Including in the future the upgraded AugerPrime detectors opens up possibilities for even improved reconstructions.

References

[1] A. Aab et al. [Pierre Auger Coll.], Nucl. Instrum. Meth. A **798** (2015) 172.
[2] A. Aab et al. [Pierre Auger Coll.], Phys. Rev. D **90** (2014) 122005.
[3] A. Abraham et al. [Pierre Auger Coll.], Phys. Rev. Lett., **104** (2010) 091101.
[4] P. Lipari, Phys. Rev. D **79** (2009) 063001.
[5] M. Ave, R. Engel, M. Roth, A. Schulz, Astropart. Phys. **87** (2017) 23.
[6] A. Bridgeman for the Pierre Auger Coll., PoS, **323** (2017) .
[7] A. Aab et al. [Pierre Auger Coll.], Phys. Rev. D **96** (2017) 122003.
[8] C. J. T. Peixoto for the Pierre Auger Coll., PoS, **440** (2019) .
[9] M. Erdmann, J. Glombitza, D. Walz, Astropart. Phys. **97** (2018) 46.
[10] A. Aab et al. [Pierre Auger Coll.], JINST **16** (2021) P07019.
[11] A. Aab et al. [Pierre Auger Coll.], JINST **15** (2020) P10021.
[12] D. Heck et al., Forschungszentrum Karlsruhe Report FZKA (1998) 6019.
[13] T. Pierog et al., Phys. Rev. D **92** (2015) 034906.
[14] S. Ostapchenko, Phys. Rev. D **72** (2006) 14.
[15] F. Riehn et al., PoS, **301** (2018).
[16] S. Agostinelli et al., Nucl. Instrum. Meth. A **506** (2003) 250.
[17] S. Argiro et al., Nucl. Instrum. Meth. A **580** (2007) 1485.
[18] S. Hochreiter, J. Schmidhuber, Neural Computation **9(8)** (1997) 1735–1780.
[19] E. Hoogeboom, J.W.T. Peters, T.S. Cohen, M. Welling, [1803.02108].
[20] F. Chollet et al., https://keras.io.
[21] M. Abadi et al., https://tensorflow.org.
[22] P. Abreu et al. [Pierre Auger Coll.], [1107.4806].
[23] A. Aab et al. [Pierre Auger Coll.], Phys. Rev. D **91** (2015) 032003.
[24] A. Aab et al. [Pierre Auger Coll.], Phys. Rev. D **90** (2014) 012012.

The Pierre Auger Collaboration

P. Abreu[72], M. Aglietta[54,52], J.M. Albury[13], I. Allekotte[1], A. Almela[8,12], J. Alvarez-Muñiz[79], R. Alves Batista[80], G.A. Anastasi[63,52], L. Anchordoqui[87], B. Andrada[8], S. Andringa[72], C. Aramo[50], P.R. Araújo Ferreira[42], J. C. Arteaga Velázquez[67], H. Asorey[8], P. Assis[72], G. Avila[11], A.M. Badescu[75], A. Bakalova[32], A. Balaceanu[73], F. Barbato[45,46], R.J. Barreira Luz[72], K.H. Becker[38], J.A. Bellido[13,69], C. Berat[36], M.E. Bertaina[63,52], X. Bertou[1], P.L. Biermann[b], V. Binet[6], K. Bismark[39,8], T. Bister[42], J. Biteau[37], J. Blazek[32], C. Bleve[36], M. Boháčová[32], D. Boncioli[57,46], C. Bonifazi[9,26], L. Bonneau Arbeletche[21], N. Borodai[70], A.M. Botti[8], J. Brack[d], T. Bretz[42], P.G. Brichetto Orchera[8], F.L. Briechle[42], P. Buchholz[44], A. Bueno[78], S. Buitink[15], M. Buscemi[47], M. Büsken[39,8], K.S. Caballero-Mora[66], L. Caccianiga[59,49], F. Canfora[80,81], I. Caracas[38], J.M. Carceller[78], R. Caruso[58,47], A. Castellina[54,52], F. Catalani[19], G. Cataldi[48], L. Cazon[72], M. Cerda[10], J.A. Chinellato[22], J. Chudoba[32], L. Chytka[33], R.W. Clay[13], A.C. Cobos Cerutti[7], R. Colalillo[60,50], A. Coleman[93], M.R. Coluccia[48], R. Conceição[72], A. Condorelli[45,46], G. Consolati[49,55], F. Contreras[11], F. Convenga[56,48], D. Correia dos Santos[28], C.E. Covault[85], S. Dasso[5,3], K. Daumiller[41], B.R. Dawson[13], J.A. Day[13], R.M. de Almeida[28], J. de Jesús[8,41], S.J. de Jong[80,81], G. De Mauro[80,81], J.R.T. de Mello Neto[26,27], I. De Mitri[45,46], J. de Oliveira[18], D. de Oliveira Franco[22], F. de Palma[56,48], V. de Souza[20], E. De Vito[56,48], M. del Río[11], O. Deligny[34], L. Deval[41,8], A. di Matteo[52], C. Dobrigkeit[22], J.C. D'Olivo[68], L.M. Domingues Mendes[72], R.C. dos Anjos[25], D. dos Santos[28], M.T. Dova[4], J. Ebr[32], R. Engel[39,41], I. Epicoco[56,48], M. Erdmann[42], C.O. Escobar[a], A. Etchegoyen[8,12], H. Falcke[80,82,81], J. Farmer[92], G. Farrar[90], A.C. Fauth[22], N. Fazzini[a], F. Feldbusch[40], F. Fenu[54,52], B. Fick[89], J.M. Figueira[8], A. Filipčič[77,76], T. Fitoussi[41], T. Fodran[80], M.M. Freire[6], T. Fujii[92,e], A. Fuster[8,12], C. Galea[80], C. Galelli[59,49], B. García[7], A.L. Garcia Vegas[42], H. Gemmeke[40], F. Gesualdi[8,41], A. Gherghel-Lascu[73], P.L. Ghia[34], U. Giaccari[80], M. Giammarchi[49], J. Glombitza[42], F. Gobbi[10], F. Gollan[8], G. Golup[1], M. Gómez Berisso[1], P.F. Gómez Vitale[11], J.P. Gongora[11], J.M. González[1], N. González[14], I. Goos[1,41], D. Góra[70], A. Gorgi[54,52], M. Gottowik[38], T.D. Grubb[13], F. Guarino[60,50], G.P. Guedes[23], E. Guido[52,63], S. Hahn[41,8], P. Hamal[32], M.R. Hampel[8], P. Hansen[4], D. Harari[1], V.M. Harvey[13], A. Haungs[41], T. Hebbeker[42], D. Heck[41], G.C. Hill[13], C. Hojvat[a], J.R. Hörandel[80,81], P. Horvath[33], M. Hrabovský[33], T. Huege[41,15], A. Insolia[58,47], P.G. Isar[74], P. Janecek[32], J.A. Johnsen[86], J. Jurysek[32], A. Kääpä[38], K.H. Kampert[38], N. Karastathis[41], B. Keilhauer[41], J. Kemp[42], A. Khakurdikar[80], V.V. Kizakke Covilakam[8,41], H.O. Klages[41], M. Kleifges[40], J. Kleinfeller[10], M. Köpke[39], N. Kunka[40], B.L. Lago[17], R.G. Lang[20], N. Langner[42], M.A. Leigui de Oliveira[24], V. Lenok[41], A. Letessier-Selvon[35], I. Lhenry-Yvon[34], D. Lo Presti[58,47], L. Lopes[72], R. López[64], L. Lu[94], Q. Luce[39], J.P. Lundquist[76], A. Machado Payeras[22], G. Mancarella[56,48], D. Mandat[32], B.C. Manning[13], J. Manshanden[43], P. Mantsch[a], S. Marafico[34], A.G. Mariazzi[4], I.C. Mariş[14], G. Marsella[61,47], D. Martello[56,48], S. Martinelli[41,8], O. Martínez Bravo[64], M. Mastrodicasa[57,46], H.J. Mathes[41], J. Matthews[88], G. Matthiae[62,51], E. Mayotte[38], P.O. Mazur[a], G. Medina-Tanco[68], D. Melo[8], A. Menshikov[40], K.-D. Merenda[86], S. Michal[33], M.I. Micheletti[6], L. Miramonti[59,49], S. Mollerach[1], F. Montanet[36], C. Morello[54,52], M. Mostafá[91], A.L. Müller[8], M.A. Muller[22], K. Mulrey[15], R. Mussa[52], M. Muzio[90], W.M. Namasaka[38], A. Nasr-Esfahani[38], L. Nellen[68], M. Niculescu-Oglinzanu[73], M. Niechciol[44], D. Nitz[89], D. Nosek[31], V. Novotny[31], L. Nožka[33], A Nucita[56,48], L.A. Núñez[30], M. Palatka[32], J. Pallotta[2], P. Papenbreer[38], G. Parente[79], A. Parra[64], J. Pawlowsky[38], M. Pech[32], F. Pedreira[79], J. Pękala[70], R. Pelayo[65], J. Peña-Rodriguez[30], E.E. Pereira Martins[39,8], J. Perez Armand[21], C. Pérez Bertolli[8,41], M. Perlin[8,41], L. Perrone[56,48], S. Petrera[45,46], T. Pierog[41], M. Pimenta[72], V. Pirronello[58,47], M. Platino[8], B. Pont[80], M. Pothast[81,80], P. Privitera[92], M. Prouza[32], A. Puyleart[89], S. Querchfeld[38], J. Rautenberg[38], D. Ravignani[8], M. Reininghaus[41,8], J. Ridky[32], F. Riehn[72], M. Risse[44], V. Rizi[57,46], W. Rodrigues de Carvalho[21], J. Rodriguez Rojo[11], M.J. Roncoroni[8], S. Rossoni[43], M. Roth[41], E. Roulet[1], A.C. Rovero[5], P. Ruehl[44], A. Saftoiu[73], F. Salamida[57,46], H. Salazar[64], G. Salina[51], J.D. Sanabria Gomez[30], F. Sánchez[8], E.M. Santos[21], E. Santos[32], F. Sarazin[86], R. Sarmento[72], C. Sarmiento-Cano[8], R. Sato[11],

P. Savina[56,48,34,94], C.M. Schäfer[41], V. Scherini[56,48], H. Schieler[41], M. Schimassek[39,8], M. Schimp[38], F. Schlüter[41,8], D. Schmidt[39], O. Scholten[84,15], P. Schovánek[32], F.G. Schröder[93,41], S. Schröder[38], J. Schulte[42], S.J. Sciutto[4], M. Scornavacche[8,41], A. Segreto[53,47], S. Sehgal[38], R.C. Shellard[16], G. Sigl[43], G. Silli[8,41], O. Sima[73,f], R. Šmída[92], P. Sommers[91], J.F. Soriano[87], J. Souchard[36], R. Squartini[10], M. Stadelmaier[41,8], D. Stanca[73], S. Stanič[76], J. Stasielak[70], P. Stassi[36], A. Streich[39,8], M. Suárez-Durán[14], T. Sudholz[13], T. Suomijärvi[37], A.D. Supanitsky[8], Z. Szadkowski[71], A. Tapia[29], C. Taricco[63,52], C. Timmermans[81,80], O. Tkachenko[41], P. Tobiska[32], C.J. Todero Peixoto[19], B. Tomé[72], Z. Torrès[36], A. Travaini[10], P. Travnicek[32], C. Trimarelli[57,46], M. Tueros[4], R. Ulrich[41], M. Unger[41], L. Vaclavek[33], M. Vacula[33], J.F. Valdés Galicia[68], L. Valore[60,50], E. Varela[64], A. Vásquez-Ramírez[30], D. Veberič[41], C. Ventura[27], I.D. Vergara Quispe[4], V. Verzi[51], J. Vicha[32], J. Vink[83], S. Vorobiov[76], H. Wahlberg[4], C. Watanabe[26], A.A. Watson[c], M. Weber[40], A. Weindl[41], L. Wiencke[86], H. Wilczyński[70], M. Wirtz[42], D. Wittkowski[38], B. Wundheiler[8], A. Yushkov[32], O. Zapparrata[14], E. Zas[79], D. Zavrtanik[76,77], M. Zavrtanik[77,76], L. Zehrer[76]

———— • ————

[1] Centro Atómico Bariloche and Instituto Balseiro (CNEA-UNCuyo-CONICET), San Carlos de Bariloche, Argentina
[2] Centro de Investigaciones en Láseres y Aplicaciones, CITEDEF and CONICET, Villa Martelli, Argentina
[3] Departamento de Física and Departamento de Ciencias de la Atmósfera y los Océanos, FCEyN, Universidad de Buenos Aires and CONICET, Buenos Aires, Argentina
[4] IFLP, Universidad Nacional de La Plata and CONICET, La Plata, Argentina
[5] Instituto de Astronomía y Física del Espacio (IAFE, CONICET-UBA), Buenos Aires, Argentina
[6] Instituto de Física de Rosario (IFIR) – CONICET/U.N.R. and Facultad de Ciencias Bioquímicas y Farmacéuticas U.N.R., Rosario, Argentina
[7] Instituto de Tecnologías en Detección y Astropartículas (CNEA, CONICET, UNSAM), and Universidad Tecnológica Nacional – Facultad Regional Mendoza (CONICET/CNEA), Mendoza, Argentina
[8] Instituto de Tecnologías en Detección y Astropartículas (CNEA, CONICET, UNSAM), Buenos Aires, Argentina
[9] International Center of Advanced Studies and Instituto de Ciencias Físicas, ECyT-UNSAM and CONICET, Campus Miguelete – San Martín, Buenos Aires, Argentina
[10] Observatorio Pierre Auger, Malargüe, Argentina
[11] Observatorio Pierre Auger and Comisión Nacional de Energía Atómica, Malargüe, Argentina
[12] Universidad Tecnológica Nacional – Facultad Regional Buenos Aires, Buenos Aires, Argentina
[13] University of Adelaide, Adelaide, S.A., Australia
[14] Université Libre de Bruxelles (ULB), Brussels, Belgium
[15] Vrije Universiteit Brussels, Brussels, Belgium
[16] Centro Brasileiro de Pesquisas Fisicas, Rio de Janeiro, RJ, Brazil
[17] Centro Federal de Educação Tecnológica Celso Suckow da Fonseca, Nova Friburgo, Brazil
[18] Instituto Federal de Educação, Ciência e Tecnologia do Rio de Janeiro (IFRJ), Brazil
[19] Universidade de São Paulo, Escola de Engenharia de Lorena, Lorena, SP, Brazil
[20] Universidade de São Paulo, Instituto de Física de São Carlos, São Carlos, SP, Brazil
[21] Universidade de São Paulo, Instituto de Física, São Paulo, SP, Brazil
[22] Universidade Estadual de Campinas, IFGW, Campinas, SP, Brazil
[23] Universidade Estadual de Feira de Santana, Feira de Santana, Brazil
[24] Universidade Federal do ABC, Santo André, SP, Brazil
[25] Universidade Federal do Paraná, Setor Palotina, Palotina, Brazil
[26] Universidade Federal do Rio de Janeiro, Instituto de Física, Rio de Janeiro, RJ, Brazil
[27] Universidade Federal do Rio de Janeiro (UFRJ), Observatório do Valongo, Rio de Janeiro, RJ, Brazil
[28] Universidade Federal Fluminense, EEIMVR, Volta Redonda, RJ, Brazil
[29] Universidad de Medellín, Medellín, Colombia
[30] Universidad Industrial de Santander, Bucaramanga, Colombia
[31] Charles University, Faculty of Mathematics and Physics, Institute of Particle and Nuclear Physics, Prague, Czech Republic
[32] Institute of Physics of the Czech Academy of Sciences, Prague, Czech Republic

PoS(ICRC2021)359

[33] Palacky University, RCPTM, Olomouc, Czech Republic
[34] CNRS/IN2P3, IJCLab, Université Paris-Saclay, Orsay, France
[35] Laboratoire de Physique Nucléaire et de Hautes Energies (LPNHE), Sorbonne Université, Université de Paris, CNRS-IN2P3, Paris, France
[36] Univ. Grenoble Alpes, CNRS, Grenoble Institute of Engineering Univ. Grenoble Alpes, LPSC-IN2P3, 38000 Grenoble, France
[37] Université Paris-Saclay, CNRS/IN2P3, IJCLab, Orsay, France
[38] Bergische Universität Wuppertal, Department of Physics, Wuppertal, Germany
[39] Karlsruhe Institute of Technology (KIT), Institute for Experimental Particle Physics, Karlsruhe, Germany
[40] Karlsruhe Institute of Technology (KIT), Institut für Prozessdatenverarbeitung und Elektronik, Karlsruhe, Germany
[41] Karlsruhe Institute of Technology (KIT), Institute for Astroparticle Physics, Karlsruhe, Germany
[42] RWTH Aachen University, III. Physikalisches Institut A, Aachen, Germany
[43] Universität Hamburg, II. Institut für Theoretische Physik, Hamburg, Germany
[44] Universität Siegen, Department Physik – Experimentelle Teilchenphysik, Siegen, Germany
[45] Gran Sasso Science Institute, L'Aquila, Italy
[46] INFN Laboratori Nazionali del Gran Sasso, Assergi (L'Aquila), Italy
[47] INFN, Sezione di Catania, Catania, Italy
[48] INFN, Sezione di Lecce, Lecce, Italy
[49] INFN, Sezione di Milano, Milano, Italy
[50] INFN, Sezione di Napoli, Napoli, Italy
[51] INFN, Sezione di Roma "Tor Vergata", Roma, Italy
[52] INFN, Sezione di Torino, Torino, Italy
[53] Istituto di Astrofisica Spaziale e Fisica Cosmica di Palermo (INAF), Palermo, Italy
[54] Osservatorio Astrofisico di Torino (INAF), Torino, Italy
[55] Politecnico di Milano, Dipartimento di Scienze e Tecnologie Aerospaziali , Milano, Italy
[56] Università del Salento, Dipartimento di Matematica e Fisica "E. De Giorgi", Lecce, Italy
[57] Università dell'Aquila, Dipartimento di Scienze Fisiche e Chimiche, L'Aquila, Italy
[58] Università di Catania, Dipartimento di Fisica e Astronomia, Catania, Italy
[59] Università di Milano, Dipartimento di Fisica, Milano, Italy
[60] Università di Napoli "Federico II", Dipartimento di Fisica "Ettore Pancini", Napoli, Italy
[61] Università di Palermo, Dipartimento di Fisica e Chimica "E. Segrè", Palermo, Italy
[62] Università di Roma "Tor Vergata", Dipartimento di Fisica, Roma, Italy
[63] Università Torino, Dipartimento di Fisica, Torino, Italy
[64] Benemérita Universidad Autónoma de Puebla, Puebla, México
[65] Unidad Profesional Interdisciplinaria en Ingeniería y Tecnologías Avanzadas del Instituto Politécnico Nacional (UPIITA-IPN), México, D.F., México
[66] Universidad Autónoma de Chiapas, Tuxtla Gutiérrez, Chiapas, México
[67] Universidad Michoacana de San Nicolás de Hidalgo, Morelia, Michoacán, México
[68] Universidad Nacional Autónoma de México, México, D.F., México
[69] Universidad Nacional de San Agustin de Arequipa, Facultad de Ciencias Naturales y Formales, Arequipa, Peru
[70] Institute of Nuclear Physics PAN, Krakow, Poland
[71] University of Łódź, Faculty of High-Energy Astrophysics,Łódź, Poland
[72] Laboratório de Instrumentação e Física Experimental de Partículas – LIP and Instituto Superior Técnico – IST, Universidade de Lisboa – UL, Lisboa, Portugal
[73] "Horia Hulubei" National Institute for Physics and Nuclear Engineering, Bucharest-Magurele, Romania
[74] Institute of Space Science, Bucharest-Magurele, Romania
[75] University Politehnica of Bucharest, Bucharest, Romania
[76] Center for Astrophysics and Cosmology (CAC), University of Nova Gorica, Nova Gorica, Slovenia
[77] Experimental Particle Physics Department, J. Stefan Institute, Ljubljana, Slovenia
[78] Universidad de Granada and C.A.F.P.E., Granada, Spain
[79] Instituto Galego de Física de Altas Enerxías (IGFAE), Universidade de Santiago de Compostela, Santiago de Compostela, Spain

PoS(ICRC2021)359

[80] IMAPP, Radboud University Nijmegen, Nijmegen, The Netherlands
[81] Nationaal Instituut voor Kernfysica en Hoge Energie Fysica (NIKHEF), Science Park, Amsterdam, The Netherlands
[82] Stichting Astronomisch Onderzoek in Nederland (ASTRON), Dwingeloo, The Netherlands
[83] Universiteit van Amsterdam, Faculty of Science, Amsterdam, The Netherlands
[84] University of Groningen, Kapteyn Astronomical Institute, Groningen, The Netherlands
[85] Case Western Reserve University, Cleveland, OH, USA
[86] Colorado School of Mines, Golden, CO, USA
[87] Department of Physics and Astronomy, Lehman College, City University of New York, Bronx, NY, USA
[88] Louisiana State University, Baton Rouge, LA, USA
[89] Michigan Technological University, Houghton, MI, USA
[90] New York University, New York, NY, USA
[91] Pennsylvania State University, University Park, PA, USA
[92] University of Chicago, Enrico Fermi Institute, Chicago, IL, USA
[93] University of Delaware, Department of Physics and Astronomy, Bartol Research Institute, Newark, DE, USA
[94] University of Wisconsin-Madison, Department of Physics and WIPAC, Madison, WI, USA

—

[a] Fermi National Accelerator Laboratory, Fermilab, Batavia, IL, USA
[b] Max-Planck-Institut für Radioastronomie, Bonn, Germany
[c] School of Physics and Astronomy, University of Leeds, Leeds, United Kingdom
[d] Colorado State University, Fort Collins, CO, USA
[e] now at Hakubi Center for Advanced Research and Graduate School of Science, Kyoto University, Kyoto, Japan
[f] also at University of Bucharest, Physics Department, Bucharest, Romania

PoS(ICRC2021)359